

A charge-insensitive single-atom spin-orbit qubit in silicon

J. Salfi,^{1,2} J. A. Mol,^{1,2} D. Culcer,¹ and S. Rogge^{1,2}

¹*School of Physics, The University of New South Wales, Sydney, NSW 2052, Australia.*

²*Centre for Quantum Computation and Communication Technology,
The University of New South Wales, Sydney, NSW 2052, Australia.*

(Dated: May 16, 2022)

High-fidelity two-qubit entanglement operations pose new challenges for spin qubits. Although spin orbit-coupling (SOC) can simplify entangling operations via coupling to electric fields and microwave photons, it exposes conventional spin qubits to electrical noise. Here we devise a gate-tunable single-acceptor spin-orbit qubit in silicon having a sweet spot where the electric dipole spin resonance (EDSR) is maximized, and the qubit is simultaneously insensitive to dephasing from low-frequency electrical noise. The sweet spot protects the qubit during rapid single-qubit EDSR and two-qubit dipole-dipole mediated operations, and is only obtained by treating SOC non-perturbatively. More than 10^4 one-qubit and 10^3 two-qubit operations are possible in the predicted relaxation time, as necessary for surface codes. Moreover, circuit quantum electrodynamics with single dopants is feasible in this scheme, including dispersive single-spin readout, cavity-mediated two-qubit entanglement, and strong Jaynes-Cummings coupling. Our approach provides a scalable route for controlling electrical and photon-mediated interactions between spins of individual dopants in silicon.

Spin qubits are important systems for quantum technologies due to their long coherence times¹⁻⁷. Two-spin entanglement poses new challenges, since exchange-based two-qubit gates are vulnerable to dephasing by electrical fluctuations^{8,9} and work only for nearest neighbours, while spin qubits couple weakly to photons. Prospects for entangling spin qubits could be boosted, especially for single atom qubits^{2,6}, by coupling of spins to electric fields, photons, or phonons¹⁰⁻²⁴, by *e.g.*, spin-orbit coupling (SOC)¹⁰⁻²⁰. However, spin-orbit qubits are vulnerable to decoherence from electrical noise^{25,26} and spin qubits with weak SOC have superior coherence^{6,7}. This raises the question, does increasing SOC necessarily enhance dephasing by electrical noise, and can it improve the number of single-qubit and two-qubit operations in the qubit lifetime?

Here we devise a long-lived hole-based spin-orbit qubit using a single acceptor dopant atom in silicon where increasing the SOC with a gate can nullify dephasing by electric-field fluctuations, at a “sweet spot” where the electric dipole spin resonance (EDSR) is simultaneously maximized. These results, which can only be obtained by treating SOC non-perturbatively, rely on a uniformly strained substrate, and a dielectric interface/gate that breaks inversion symmetry, confines the light holes (LH), and couples the LH and heavy-hole (HH) manifolds.

The gate and interface strongly enhance EDSR relative to a bulk acceptor, while the sweet spot protects coherence during electrically mediated single qubit and two-qubit gates^{23,27,28}, and the LH-HH splitting enhances the qubit lifetime relative to a bulk acceptor^{29,30}. The achieved EDSR coupling allows for single-qubit gates with 0.2 ns gate times, and $> 10^4$ operations in the predicted lifetime. Two-qubit entanglement based on spin-dependent electric dipole-dipole interactions^{10,11,31} is feasible with $\sqrt{\text{SWAP}}$ times of 2 ns and $> 10^3$ operations in the predicted lifetime, for 20 nm acceptor separa-

tions. Finally, EDSR interactions enable circuit quantum electrodynamics^{32,33} (cQED) with single-spin dispersive readout, and long distance spin-spin entanglement with $\sqrt{\text{SWAP}}$ times of 200 ns. On resonance, strong single spin-photon coupling with $g_c = 5$ MHz is feasible.

Our qubit combines several desirable properties: it has a long lifetime, has fast operations, is based on a single atom, and offers long-range qubit coupling. Decoherence from host crystal nuclear spins will be suppressed for holes³⁴, or could be virtually eliminated by using ²⁸Si³⁵. The acceptor ion plays a key role by enabling LH-HH coupling^{29,30,36,37} from which the sweet spot arises under non-perturbative conditions. The single-atom confinement simplifies operation relative to multi-quantum dot systems, which require complex gates.

Device. The qubit is the spin of a hole bound to a single B:Si dopant, either implanted, or patterned by scanning tunneling microscopy in silicon-on-insulator (SOI) near an interface (Fig. 1A). Biaxial tensile strain in the SOI produces a LH ground state, quantizing spin along the z axis^{29,30}. Biasing gates relative to the handling wafer adjusts the gate electric field $\hat{z}E_z$ and applies oscillating in-plane fields for EDSR. Zeeman interactions with in-plane magnetic fields $\hat{y}B_0$ avoid dissipative losses for superconducting cQED. In contrast to previously proposed acceptor qubits employing elastic (phonon) couplings^{16,38}, our B:Si qubit couples via electric fields and microwave photons, due to gate-tunable inversion symmetry breaking.

Acceptor Hamiltonian and eigenstates. Acceptor bound-holes can be described by the Luttinger Kohn (LK) Hamiltonian $H(\mathbf{k})$ for a hole in a bulk crystal³⁹ and the ion potential $H_{\text{ion}} = e^2/(4\pi\epsilon r)$, where \mathbf{r} is the hole position and ϵ is the permittivity^{29,39}. The ground state $|\Psi_{m_J}\rangle$ is fourfold degenerate, with HH ($m_J = \pm\frac{3}{2}$) and LH ($m_J = \pm\frac{1}{2}$) eigenstates composed mainly of $|J = \frac{3}{2}, m_J\rangle$ Bloch states²⁹. A B:Si acceptor has a binding energy $E_i = 46$ meV which is isolated by > 20 meV

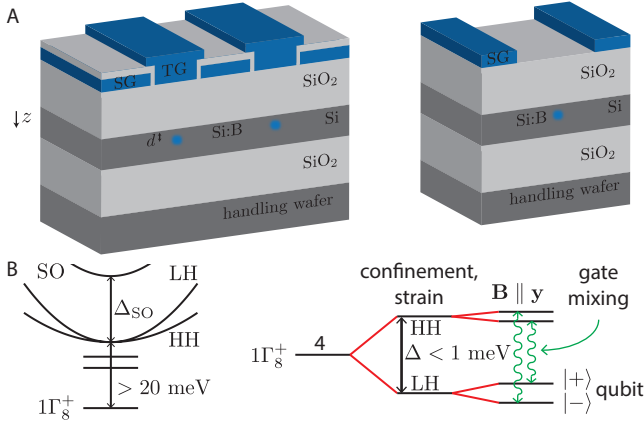


FIG. 1. A. Device schematic, showing near-interface B:Si spin qubits with gates to SG and TG to apply in-plane and vertical electric fields, respectively (left), or for cQED, gates forming the resonator apply both the in-plane and vertical electric fields (right). B. Electronic structure of an acceptor, where the LH-HH splitting Δ is determined by the strain, interface, and gate field E_z , while E_z also creates a LH-HH mixing.

relative to the first excited state⁴⁰.

Interactions with magnetic fields \mathbf{B} and strains ϵ_{ij} are represented by $H_Z = \mu_B(g_1(J_x B_x + \text{c.p.}) + g_2(J_x^3 B_x + \text{c.p.}))$ and $H_\epsilon = a' \text{Tr}[\epsilon] + b'(J_x^2 - \frac{5}{4}I)\epsilon_{xx} + \text{c.p.}) + (2d'/\sqrt{3})(\{J_x, J_y\}\epsilon_{xy} + \text{c.p.})$, respectively, in the $|\Psi_{m_J}\rangle$ subspace. Here, $\{J_x, J_y\} = \frac{1}{2}(J_x J_y + J_y J_x)$, J_α are $J = 3/2$ Pauli matrices, g_1 and g_2 are the linear and cubic g-factors, a' , b' and d' are Bir-Pikus deformation potentials, and μ_B is the Bohr magneton²⁹.

Interactions with electric fields \mathbf{E} arise from two mechanisms. First, the dopant ion's local field has T_d symmetry, and its interaction $H_{E,\text{ion}} = 2p/\sqrt{3}(E_x\{J_x, J_y\} + \text{c.p.})$ is linear in electric fields, where p , known from experiments^{36,37}, reflects the electron density near the ion³⁰. A second-order interaction $H_E = -(aE^2I + b((J_x^2 - \frac{5}{4}I)E_x^2 + \text{c.p.}) + (2d/\sqrt{3})(\{J_x, J_y\}E_x E_y + \text{c.p.}))$ ³⁰ arises from broken inversion symmetry.

In our qubit, interactions $H_{\text{if}} = U_0\Theta(-z)$ with the interface and ezE_z with the gate field break inversion symmetry, where U_0 and Θ are the barrier strength and Heaviside step function, respectively. We determine the form of H_{if} and H_E using the spherical spin-3/2 basis⁴¹ (see Appendix IA). These states satisfy $\langle \Psi_{m_J} | H_{\text{if}} | \Psi_{m'_J} \rangle = 0$ when $m_J \neq m'_J$, since H_{if} is a function of z only. Taking the HHs as a reference, we obtain $H_{\text{if}} = \text{diag}\{0, \Delta_{\text{if}}, \Delta_{\text{if}}, 0\}$; the light holes are confined, as for a two dimensional hole gas⁴². The potential of the gate field is also a function of z only, such that $H_{E_z} = \text{diag}\{0, \Delta_G(E_z), \Delta_G(E_z), 0\}$. Following ref. 29, we use $H_{E_\parallel} = \alpha(E_z)(\{J_y, J_z\}E_y + \{J_z, J_x\}E_x)$ for the second order interaction involving in-plane fields $E_{x,y}$ and the inversion symmetry breaking potential of the gate/interface, encapsulated in $\alpha(E_z)$.

Parameters Δ_{if} , $\Delta_G(E_z)$, and $\alpha(E_z)$ were computed numerically in the 6×6 LK representation³⁹. These cal-

culations also verified that within the 4×4 subspace, H_{if} and H_E in the spherical spin-3/2 basis have the same symmetry as the full 6×6 LK Hamiltonian. The latter includes the cubic LK term, the split-off (SO) holes (see Fig. 1B), and inversion asymmetry-induced hybridization of levels outside the 4×4 subspace. A full numerical solution (including renormalized Zeeman interactions explicitly neglected in our analytic model) is also presented.

The LH ground state is obtained using biaxial tensile strain ϵ_\parallel in SOI when $\Delta_\epsilon = -2b'(2C_{12}/C_{11} + 1)\epsilon_\parallel > \Delta_{\text{if}}$ (C_{ij} are elastic moduli⁴³), since $H_{\epsilon,\text{biax.}} = \frac{1}{2} \text{diag}\{\Delta_\epsilon, -\Delta_\epsilon, -\Delta_\epsilon, \Delta_\epsilon\}$. Recently, Δ_{if} up to 5 meV has been measured for B:Si near vacuum interfaces⁴⁴. Using $b' = -1.42$ eV, $C_{11} = 160$ GPa and $C_{12} = 58$ GPa for Si, $\Delta_{\text{if}} < 5$ meV is obtained for $\epsilon_\parallel < 0.1\%$ larger than unintentional strains in recent work^{45,46}.

Operating point and sweet spot. The gate field $\hat{z}E_z$ defines the operating point, and a sweet spot occurs when the Larmor frequency is insensitive to fluctuations $\delta\mathbf{E} = \hat{x}\delta E_x + \hat{y}\delta E_y + \hat{z}\delta E_z$. At an operating point, the qubit is described in the basis $\{|\Psi_{m_J}\rangle\}$ by

$$H_{\text{op}} = \begin{pmatrix} 0 & -i\frac{\sqrt{3}}{2}\epsilon_Z & -ipE_z & 0 \\ i\frac{\sqrt{3}}{2}\epsilon_Z & \Delta(E_z) & -i\epsilon_Z & -ipE_z \\ ipE_z & i\epsilon_Z & \Delta(E_z) & -i\frac{\sqrt{3}}{2}\epsilon_Z \\ 0 & ipE_z & i\frac{\sqrt{3}}{2}\epsilon_Z & 0 \end{pmatrix} \quad (1)$$

for $m_J = +\frac{3}{2}, +\frac{1}{2}, -\frac{1}{2}, -\frac{3}{2}$, where $\epsilon_Z = g_1\mu_B B$ and $\Delta(E_z) = -\Delta_\epsilon + \Delta_{\text{if}} + \Delta_G(E_z)$. Since $g_1/g_2 \gg 1$ for B:Si^{36,47}, we assume $g_2 = 0$ in the analytic model.

Inspecting Eq. 1, there is an avoided crossing $2pE_z$ for the LHs and HHs at $\Delta(E_z) = 0$ when gate confinement compensates strain ($\Delta_G(E_z) + \Delta_{\text{if}} = \Delta_\epsilon$), and $\epsilon_Z = 0$. For an anticrossing at $E_z \sim 15$ MV/m that we will show can be obtained for near-interface Si acceptors, $\epsilon_Z/2pE_z \sim 1/10$ for $B_0 \sim 0.5$ T, where $p = 0.26$ Debye (1 Debye ≈ 0.021 e.nm) and B:Si³⁶. Consequently, the SOC term pE_z is treated exactly and ϵ_Z by successive approximations, which we later compare with an exact solution of Eq. 1. We begin in a basis that diagonalizes H_{op} assuming $\epsilon_Z = 0$, consisting of low energy hole spins $|\pm\rangle = a_L |\Psi_{\pm 1/2}\rangle \pm ia_H |\Psi_{\mp 3/2}\rangle$ with energies $\epsilon_l = \frac{1}{2}(\Delta - \sqrt{\Delta^2 + 4E_z^2 p^2})$, and upper branch hole spins $|u\pm\rangle = a_L |\Psi_{\pm 3/2}\rangle \mp ia_H |\Psi_{\mp 1/2}\rangle$ with energies $\epsilon_u = \frac{1}{2}(\Delta + \sqrt{\Delta^2 + 4E_z^2 p^2})$. Here, $a_L = \epsilon_l/\sqrt{E_z^2 p^2 + \epsilon_l^2}$ and $a_H = \sqrt{1 - a_L^2} = E_z p/\sqrt{E_z^2 p^2 + \epsilon_l^2}$.

Rotating H_{op} into the basis $\{-, +, u-, u+\}$ we obtain

$$\bar{H}_{\text{op}} = \begin{pmatrix} \epsilon_l & \frac{1}{2}\lambda_{Zl}^* & \frac{1}{2}\lambda_{Zo}^* & 0 \\ \frac{1}{2}\lambda_{Zl} & \epsilon_l & 0 & \frac{1}{2}\lambda_{Zo} \\ \frac{1}{2}\lambda_{Zo} & 0 & \epsilon_u & \frac{1}{2}\lambda_{Zu}^* \\ 0 & \frac{1}{2}\lambda_{Zo}^* & \frac{1}{2}\lambda_{Zu} & \epsilon_u \end{pmatrix}, \quad (2)$$

where the effective Zeeman interactions $\lambda_{Zl} = 2\epsilon_Z(\sqrt{3}a_L a_H - ia_L^2)$, $\lambda_{Zu} = 2\epsilon_Z(\sqrt{3}a_L a_H - ia_H^2)$, and $\lambda_{Zo} = 2\epsilon_Z(-a_H a_L + i\sqrt{3}a_L^2/2 - i\sqrt{3}a_H^2/2)$ explicitly depend on the gate-induced LH-HH mixing.

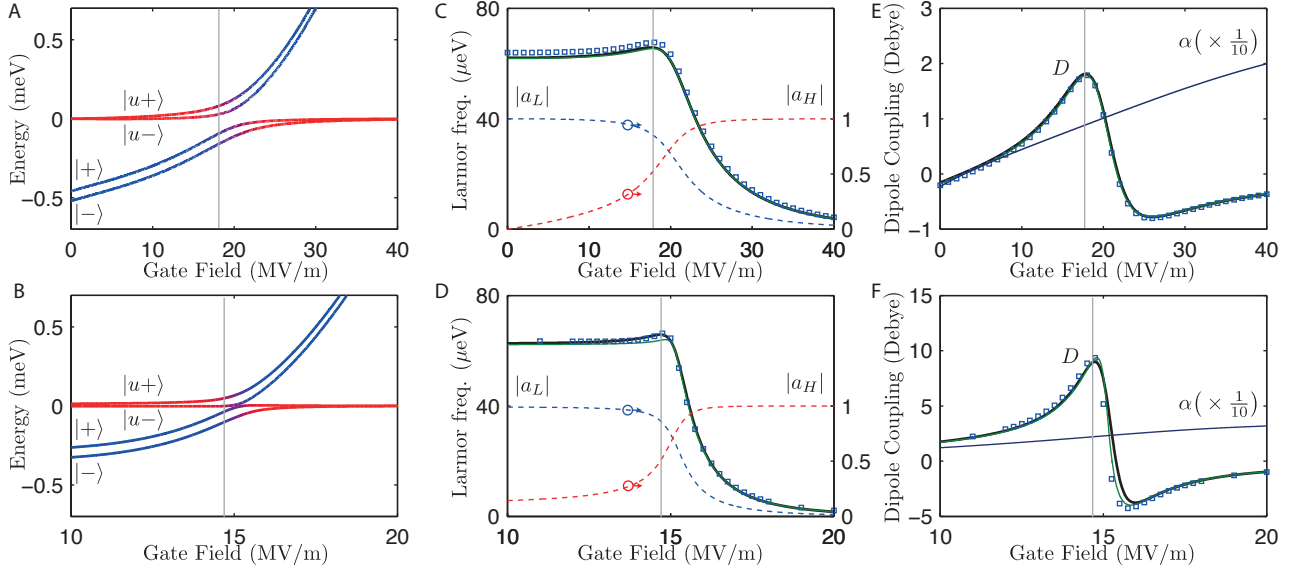


FIG. 2. Spin qubit levels ε_{\pm} and upper branch levels $\varepsilon_{u\pm}$ for (A) $d = 4.6$ nm and (B) $d = 6.9$ nm, using approximate model. Larmor frequencies for (C) $d = 4.6$ nm and (D) $d = 6.9$ nm using approximate model (black), analytic model (green), and numerical (blue squares) solutions. Spectral weights $|a_L|$ (blue dashed) and $|a_H|$ (red dashed) for $|\pm\rangle$ are also shown. Predicted EDSR coupling D in the qubit subspace for (E) $d = 4.6$ nm and (F) $d = 6.9$ nm, for approximate model (black), analytic model (green), and numerical solution (blue squares), with α (blue) determined from numerics. We take $B_0 = 0.5$ T, $\Delta_{\varepsilon} = 0.62$ meV for $d = 4.6$ nm, and $\Delta_{\varepsilon} = 0.34$ meV for $d = 6.9$ nm.

As we now show, the E_z dependence of the qubit Larmor frequency $\hbar\omega$ has a sweet spot, to zeroth order in λ_{Z_0} . Moreover, for $2pE_z/\varepsilon_Z \sim 10$, the lowest non-zero correction is to 2nd order in $\lambda_{Z_0}/(\varepsilon_u - \varepsilon_l)$, and does not qualitatively change the behaviour of the sweet spot (see Appendix I C). At $B_0 = 0.5$ T we obtain $2pE_z/\varepsilon_Z \sim 10$ at $E_z \sim 15$ MV/m. While this E_z is larger than the ionization field of B:Si in bulk silicon⁴⁸, the interface prevents ionization in our device. Taking this approach, $\hbar\omega \approx |\lambda_{Zl}| = 2\varepsilon_Z \sqrt{3a_L^2 a_H^2 + a_L^4}$, and a sweet spot occurs at the roots of $\partial\hbar\omega/\partial E_z = 2\varepsilon_Z (\partial a_L/\partial E_z)(3 - 4a_L^2)/\sqrt{3 - 2a_L^2}$. One sweet spot is $(a_L, a_H) = (-\frac{\sqrt{3}}{2}, \frac{1}{2})$, where the qubit is mostly LH-like. Substituting ε_l and $\Delta(E_z)$, we obtain $\Delta_G(E_z) + \Delta_{if} + 2p/\sqrt{3}E_z = \Delta_{\varepsilon}$ for this sweet spot. A second sweet spots occurs when $\partial a_L/\partial E_z = E_z^2 p^2 (\partial \varepsilon_l/\partial E_z)(\varepsilon_l^2 + E_z^2 p^2)^{-3/2} = 0$, at $E_z = 0$. Note that $\partial\hbar\omega/\partial \delta E_{x,y} = 0$ for any operating point. In the remainder of the paper, we focus on the properties of the “finite-field” sweet spot at $(a_L, a_H) = (-\frac{\sqrt{3}}{2}, \frac{1}{2})$, where EDSR should be possible due to inversion symmetry breaking.

Energy levels $\varepsilon_{\pm} = \varepsilon_l \pm \frac{1}{2}\hbar\omega$ and $\varepsilon_{u\pm} = \varepsilon_u \pm \frac{1}{2}|\lambda_{Zu}|$ are shown versus gate field for a $d = 4.6$ nm (6.9 nm) deep acceptor, as blue-red lines in Fig. 2A (Fig. 2B), taking into account $\Delta_G(E_z)$ and the E_z dependence of p from numerical calculations. In these spectra, blue (red) color denotes the weight of the light (heavy) holes, and the LH-HH anticrossing occurs at $E_z = 20$ MV/m (15.3 MV/m) for $d = 4.6$ nm (6.9 nm). The sweet spot indicated at the maxima of $\hbar\omega$ in Fig. 2C (Fig. 2D) occurs at $E_z = 17$ MV/m (14.8 MV/m) for $d = 4.6$ nm

(6.9 nm), and as expected, for LH and HH weights in Fig. 2C (Fig. 2D), $|a_L| = \frac{\sqrt{3}}{2}$ and $|a_H| = \frac{1}{2}$. The analytic solution of the Larmor frequency (green) is shown alongside the numerical solution (blue squares), demonstrating that the approximate solution accounts for the essential behaviour. Corrections to the Zeeman interaction included in the numerics, including the cubic term and asymmetry-induced mixing from outside of the 4×4 subspace, are therefore very small.

Electric dipole spin resonance. In the $\{-, +, u-, u+\}$ basis, interactions with in-plane electric fields E_x and E_y are described by

$$\tilde{H} = \begin{pmatrix} \varepsilon_l - \frac{\hbar\omega}{2} & 0 & E_1 + Z_1 & E_2 + Z_2 \\ 0 & \varepsilon_l + \frac{\hbar\omega}{2} & E_2 + Z_2 & E_1 + Z_1 \\ E_1^* + Z_1^* & E_2^* + Z_2^* & \varepsilon_u - \frac{|\lambda_{Zu}|}{2} & 0 \\ E_2^* + Z_2^* & E_1^* + Z_1^* & 0 & \varepsilon_u + \frac{|\lambda_{Zu}|}{2} \end{pmatrix}. \quad (3)$$

Here, $Z_1 = \frac{1}{2}\varepsilon_{Z_0} \cos(\theta_l/2 - \theta_u/2 - \theta_o)$, $Z_2 = \frac{1}{2}\varepsilon_{Z_0} i \sin(\theta_l/2 - \theta_u/2 - \theta_o)$, $E_1 = i(\alpha \sin \theta + p \cos \theta)E_x + i(\alpha \cos \theta + p \sin \theta)E_y$, $E_2 = (-\alpha \cos \theta + p \sin \theta)E_x + (\alpha \sin \theta - p \cos \theta)E_y$, $\theta = \theta_u - \theta_l$, and $|E_{Zi}| \exp(i\theta_i) = \lambda_{Zi}$.

A Schrieffer-Wolff (SW) transformation^{42,49} was used to obtain the EDSR coupling in the qubit subspace $|\pm\rangle$ due to in-plane fields $\mathbf{E}_{\parallel} = E_{\parallel}(\hat{x} \cos \theta_{\parallel} + \hat{y} \sin \theta_{\parallel})$. We obtain $D = \varepsilon_{Z_0}(\varepsilon_l - \varepsilon_u)^{-1}(\alpha \cos(\theta_o - \theta_{\parallel}) + p \sin(\theta_o - \theta_{\parallel}))$ in $\tilde{H}_{\text{EDSR}} = DE_{\parallel} \sigma_x$ (see Appendix I D). Here, the second-order LH-HH couplings $\alpha E_{x,y}$ due to inversion symmetry breaking by the interface and gate are 100 times stronger than $pE_{x,y}$, since as shown for $d = 4.6$ nm (6.9 nm) in Fig. 2E (Fig. 2F), $\alpha \approx 25$ Debye are obtained, while

$p = 0.26$ Debye is well-known for B:Si³⁶.

The EDSR strength D and gate fidelity can be optimized via the orientation of \mathbf{E}_{\parallel} relative to \mathbf{B} . Since $\alpha \sim 100p$ and $\theta_o = \pi/4$ at the sweet spot, D is maximized with respect to θ_{\parallel} at $\theta_{\parallel} = -\pi/4 \pm \pi/2$. More subtly, D is also maximized with respect to E_z at the sweet spot for $\theta_{\parallel} = -\pi/4 \pm \pi/2$, as shown for $d = 4.6$ nm ($d = 6.9$ nm) in Fig. 2E (Fig. 2F) with $\theta_{\parallel} = \pi/4$, a result that can be easily obtained analytically, and in agreement with the analytic (green) and numerical (blue squares) solutions. This means that increasing SOC towards the sweet spot both enhances EDSR, and as previous discussed, reduces sensitivity to noise. Since D is maximized at the sweet spot, the fidelity of EDSR operations will be protected from electrical noise.

Qubit operation The one-qubit and two-qubit gates are performed at the sweet spot via electrical interactions where coherence and gate fidelity are protected against low-frequency electrical noise. EDSR driven π rotations can be accomplished on individual qubits on a timescale $\tau_1 = h/(2DE_{AC}) = 1$ ns (0.2 ns) for the $d = 4.6$ nm (6.9 nm) deep acceptor, assuming a modest in-plane microwave field amplitude $E_{AC} = 500$ V/cm. Rotations σ_y are work using $\pi/4$ phase shifts relative to the σ_x gate, and following magnetic resonance concepts, the σ_z gate may be a composite of σ_x and σ_y gates. Initialisation can be performed by loading into a spin eigenstate from a carrier reservoir, and/or waiting the required T_1 time. Readout can be accomplished by energy-dependent or spin-dependent tunneling^{50,51}.

Because the electric dipole moment of each hole couples to its spin, two proximate hole spins can be entangled via a spin-spin interaction mediated by electric dipole-dipole coupling^{10,11,31}. The spin-dependent dipole-dipole coupling strength is given by $J_{dd,xx} = (\mathbf{v}_1 \cdot \mathbf{v}_2 R^2 - 3(\mathbf{v}_1 \cdot \mathbf{R})(\mathbf{v}_2 \cdot \mathbf{R})) / (4\pi\epsilon R^5)$, where \mathbf{v}_i is the spin-dependent charge dipole of qubit, which has the same magnitude as the EDSR matrix element^{10,11,31}. For a 20 nm distance with negligible tunnel coupling, we obtain a $\sqrt{\text{SWAP}}$ time of $\tau_{2dd} = h/4J_{dd,xx} \approx 2$ ns since $J_{dd,xx} \approx D^2/4\pi\epsilon R^3$. Two qubit interactions may be switched on by sweeping via TG top gates (Fig.1A) both qubits to the finite field sweet spot with strong EDSR coupling and $\hbar\omega \approx 2.12\epsilon_Z$.

We remark that two-acceptor coupling by the exchange interaction is also possible, and that it is essentially hydrogenic in the present case where the desired tunnel coupling is less than the LH-HH splitting⁵². Moreover, valley-interference effects, recently observed in single donor experiments⁵³ and which may complicate exchange processes⁵⁴, are avoided in the valence band.

Cavity coupling Microwave photons in superconducting cavities could be used to implement cQED, including two-qubit gates, dispersive single-spin readout, and strong Jaynes-Cummings coupling on resonance with the cavity^{24,32,33}. We assume a coplanar waveguide resonator operating at $B = 0.5$ T ($f = 15$ GHz) with a 6 micron gap tapered to 60 nm near the dopant (see Fig. 1A left),

where SG gates also tune E_z . The taper enhances the vacuum field from E_0 from ≈ 0.5 V/m to ≈ 50 V/m, enhancing the vacuum Rabi coupling¹⁹. At the sweet spot for $d = 4.6$ nm (6.9 nm), the vacuum Rabi coupling is $g_c = DE_0 = 2$ neV (10 neV).

For non-demolition dispersive readout and long-range two-qubit coupling, we work in the regime where the acceptor spin level is detuned from the cavity by an amount $\Delta = g_c/4$, following ref. 15. In this regime, the dispersive readout shift is $\Delta f = g_c^2/\Delta = 0.25$ MHz (1.25 MHz) for the sweet spot at $d = 4.6$ nm (6.9 nm). The two-qubit $\sqrt{\text{SWAP}}$ time is $\tau_{2c} = h/4H_{ss} = 200$ ns for $d = 6.9$ nm, determined by the effective spin-spin interaction¹⁵ $J_{c,xx} = 2g_c^2/\Delta = 2.5$ MHz. Operating on resonance with the cavity, spin/photon Rabi oscillations require $\hbar\pi/g_c = 1$ μ s (200 ns). Assuming $Q = 10^5$ cavity at $B_0 = 0.5$ T in state-of-the-art superconducting resonators^{55,56} the achievable co-operativity is $W = g_c\kappa = 6.7$ (33) for $d = 4.6$ nm (6.9 nm), where $\kappa = f/Q$ is the cavity loss rate.

Relaxation and dephasing For temperatures T satisfying $kT \ll \hbar\omega$, the phonon-mediated spin relaxation is

$$\frac{1}{T_1} = \frac{(\hbar\omega)^5}{320\rho\hbar^4\pi p^2 E_z^2} \left[\frac{9b'^2}{32} \left(\frac{2}{v_l^5} + \frac{4}{3v_t^5} \right) + \frac{5d'^2}{16} \left(\frac{2}{3v_l^5} + \frac{1}{v_t^5} \right) \right] \quad (4)$$

at the sweet spot (see Appendix IE). Using $v_l = 8.99 \times 10^3$ m/s and $v_t = 1.7v_l$ for the longitudinal and transverse sound velocities, $\rho = 2330$ kg/m³ for the density, and $b' = -1.4$ eV and $d' = -3.7$ eV⁴⁷, we obtain $T_1 = 20$ μ s (5 μ s) for $d = 4.6$ nm (6.9 nm) at $B_0 = 0.5$ T. These T_1 figures are > 30 times larger than those of unstrained acceptors in bulk silicon^{16,30}.

The predicted T_1 exceeds the gate times $\tau_1 = 0.2$ ns, $\tau_{2dd} = 2$ ns and $\tau_{2c} = 200$ ns by $> 10^4$, $> 10^3$ and 25, respectively. Moreover, all of these ratios increase favourably when decreasing B , since $T_1 \propto B^{-5}$, $\tau_1 \propto B^{-1}$, $\tau_{2dd} \propto B^{-2}$, while $\tau_{2c} \propto B^{-4}$, since $E_{vac} \propto B$. For $B_0 = 0.25$ T, we obtain $T_1 = 160$ μ s, $\tau_1 = 0.4$ ns, $\tau_{2dd} = 8$ ns, and $\tau_{2c} = 3.2$ μ s for $d = 6.9$ nm.

Electrical noise from tunneling two-level systems and fluctuating charge traps⁵⁷ can cause dephasing in spin-orbit qubits²⁶. While low-temperature metrology of charge fluctuators in Si devices is an active area of research, we estimate the dephasing caused by a single fluctuator near a top gate in Figure 1A for illustrative purposes. Treating the fluctuator as a perturbation, $(T_2^*)^{-1} = (\delta\hbar\omega)^2\tau/2\hbar^2$ is obtained²⁶, where $\delta\hbar\omega$ is the Larmor energy shift due to the fluctuator (and its image charge in the gate, see Appendix IF), and τ is the switching time²⁶. Assuming a switching time $\tau = 10^3\tau_1$ and a defect laterally 40 nm away, we find a window 0.4 MV/m (0.03 MV/m) wide around the sweet spot where $T_2^* > 2T_1$ for the $d = 4.6$ nm (6.9 nm) deep acceptor. The choice $\tau = 10^3\tau_1$ is justified for a worst case estimate of T_2^* , since dephasing by slower fluctuations can be highly suppressed by EDSR-mediated dynamical decoupling.

Nuclear spin bath fluctuations of the host crystal also

cause decoherence via hyperfine interactions. However, natural silicon has only 4.7 % of spin-bearing isotopes (^{29}Si), the hyperfine interactions are weaker for holes than electrons³⁴, and isotope-purified ^{28}Si can effectively eliminate the decoherence by the nuclear bath³⁵.

Conclusions We have devised a single-atom hole spin qubit in silicon based on an acceptor near an interface where increasing SOC from a fixed point can reduce, and eliminate to first order, dephasing from electrical noise at a ‘‘sweet spot’’. The qubit EDSR response is maximized by enhancing SOC towards the sweet spot, increasing the speed of electrically mediated one and two-qubit gates. We find that $> 10^4$ single-qubit and $> 10^3$ operations are possible, respectively, in the predicted lifetime. Moreover, the EDSR coupling is sufficient to realize cQED for dispersive single-spin readout, long-distance two-qubit coupling with a 200 ns $\sqrt{\text{SWAP}}$ time, or to realize Jaynes-Cummings entanglement between single photons and single spins.

ACKNOWLEDGEMENTS

We thank R. Winkler, U. Zuelicke and M. Tong and T. Kobayashi for helpful discussions. This work was supported by the ARC Centre of Excellence for Quantum Computation and Communication Technology (CE110001027), and in part by the US Army Research Office (W911NF-08-1-0527).

I. APPENDIX

A. Acceptor states in spherical spin-3/2 basis

In the spherical spin-3/2 basis $|L, S; J, m_J\rangle$, where $\mathbf{J} = \mathbf{L} + \mathbf{S}$ is an effective total angular momentum⁴¹, acceptor eigenstates take the form

$$|\Psi_{m_J}\rangle = f_0(r) |0, \frac{3}{2}; \frac{3}{2}, m_J\rangle + g_0(r) |2, \frac{3}{2}; \frac{3}{2}, m_J\rangle, \quad (\text{A1})$$

where $S = \frac{3}{2}$ is an effective total spin, and the spin-3/2 spin-orbit interaction has coupled states with $\Delta L = 0, \pm 2$. The $f_0(r)$ and $g_0(r)$ are radial wavefunctions for angular momentum $L = 0$ and $L = 2$, respectively, and the $|L, S; J, m_J\rangle$ are found using the Clebsch-Gordan coefficients. States outside the 4×4 subspace are also given in ref. 41.

B. Unitary Transformations

The unitary transforms U_0 and U_{Z0} which diagonalize $H_{\text{op}}(\varepsilon_Z = 0)$ and $\tilde{H}_{\text{op}}(\lambda_{Z0} = 0)$ are given by

$$U_0 = \begin{pmatrix} -ia_H & 0 & 0 & a_L \\ 0 & a_L & ia_H & 0 \\ a_L & 0 & 0 & -ia_H \\ 0 & ia_H & a_L & 0 \end{pmatrix}, \quad (\text{A2})$$

in the basis $|\Psi_{m_J}\rangle$ with ordering $m_J = +\frac{3}{2}, +\frac{1}{2}, -\frac{1}{2}, -\frac{3}{2}$, where a_L and a_H are defined in the main text, and

$$U_{Z0} = 2^{-\frac{1}{2}} \begin{pmatrix} +e^{-i\theta_l/2} & +e^{-i\theta_l/2} & 0 & 0 \\ -e^{+i\theta_l/2} & +e^{+i\theta_l/2} & 0 & 0 \\ 0 & 0 & +e^{-i\theta_u/2} & +e^{-i\theta_u/2} \\ 0 & 0 & -e^{+i\theta_u/2} & +e^{+i\theta_u/2} \end{pmatrix}, \quad (\text{A3})$$

in the basis $|-\rangle, |+\rangle, |u-\rangle, |u+\rangle$ from the main text, respectively, where,

$$\theta_l = \arctan(\sqrt{3}a_H a_L, -a_L^2), \quad (\text{A4})$$

$$\theta_u = \arctan(\sqrt{3}a_L a_H, -a_H^2), \quad (\text{A5})$$

$$\varepsilon_{Zl} = 2\varepsilon_Z \sqrt{3a_L^2 a_H^2 + a_L^4}, \quad (\text{A6})$$

$$\varepsilon_{Zu} = 2\varepsilon_Z \sqrt{3a_L^2 a_H^2 + a_H^4}. \quad (\text{A7})$$

C. Response to electrical perturbations

To obtain the lowest order behaviour of λ_{Z0} it is most convenient to work with $\tilde{H}_{\text{op}} = U_{t0}^\dagger H_{\text{op}} U_{t0}$ where $U_{t0} = U_0 U_{Z0}$. Rotated into this basis we obtain

$$\tilde{H}_{\text{op}} = \begin{pmatrix} \varepsilon_l - \frac{\hbar\omega}{2} & 0 & Z_1 & Z_2 \\ 0 & \varepsilon_l + \frac{\hbar\omega}{2} & Z_2 & Z_1 \\ Z_1^* & Z_2^* & \varepsilon_u - \frac{\varepsilon_{Zu}}{2} & 0 \\ Z_2^* & Z_1^* & 0 & \varepsilon_u + \frac{\varepsilon_{Zu}}{2} \end{pmatrix} \quad (\text{A8})$$

where,

$$Z_1 = \frac{1}{2}\varepsilon_{Z0} \cos(\theta_l/2 - \theta_u/2 - \theta_o) \quad (\text{A9})$$

$$Z_2 = \frac{1}{2}\varepsilon_{Z0} i \sin(\theta_l/2 - \theta_u/2 - \theta_o) \quad (\text{A10})$$

$$\theta_o = \arctan\left(\frac{\sqrt{3}}{2}(a_L^2 - a_H^2), a_H a_L\right), \quad (\text{A11})$$

$$\varepsilon_{Z0} = 2\varepsilon_Z \sqrt{3(a_L^2 - a_H^2)^2/4 + a_H^2 a_L^2}. \quad (\text{A12})$$

The lowest order correction to $\hbar\omega$ due to coupling to levels $|u\pm\rangle$ is obtained from 2nd-order perturbation theory,

$$\hbar\omega^{(2)} = -\frac{1}{4} \left(\frac{\varepsilon_{Z0}}{\varepsilon_l - \varepsilon_u} \right)^2 (\varepsilon_{Zl} - \varepsilon_{Zu} \cos(2\theta_o - \theta_l + \theta_u)). \quad (\text{A13})$$

The exact solution in Fig. 2C,D, shows that all higher order corrections (including $\hbar\omega^{(2)}$) to the approximate solution presented in the main text do not qualitatively modify the E_z dependence of $\hbar\omega$.

D. Interaction with in-plane electric fields

In the $|\Psi_{m,j}\rangle$ basis, the total interaction with in-plane electric fields E_x and E_y described by H_E and $H_{E,\text{ion}}$ is

$$H_{E_{\parallel}} = \alpha(E_z) \begin{pmatrix} 0 & E_- & 0 & 0 \\ E_+ & 0 & 0 & 0 \\ 0 & 0 & 0 & -E_- \\ 0 & 0 & -E_+ & 0 \end{pmatrix} + p \begin{pmatrix} 0 & -iE_+ & 0 & 0 \\ iE_- & 0 & 0 & 0 \\ 0 & 0 & 0 & +iE_+ \\ 0 & 0 & -iE_- & 0 \end{pmatrix}, \quad (\text{A14})$$

where $E_+ = E_x + iE_y$ and $E_- = E_x - iE_y$. The first matrix is the coupling due to the broken inversion symmetry of the interface and gate field, along the z direction, while the second matrix describes the interaction due to the T_d symmetry of the local field of the ion. Rotated into the qubit basis using $U_{t0} = U_{Z0}U_0$, we obtain

$$\tilde{H} = \begin{pmatrix} \varepsilon_l - \frac{\hbar\omega}{2} & 0 & E_1 + Z_1 & E_2 + Z_2 \\ 0 & \varepsilon_l + \frac{\hbar\omega}{2} & E_2 + Z_2 & E_1 + Z_1 \\ E_1^* + Z_1^* & E_2^* + Z_2^* & \varepsilon_u - \frac{\varepsilon_{Zu}}{2} & 0 \\ E_2^* + Z_2^* & E_1^* + Z_1^* & 0 & \varepsilon_u + \frac{\varepsilon_{Zu}}{2} \end{pmatrix}, \quad (\text{A15})$$

where, $E_1 = i(\alpha \sin \theta + p \cos \theta)E_x + i(\alpha \cos \theta + p \sin \theta)E_y$, $E_2 = (-\alpha \cos \theta + p \sin \theta)E_x + (\alpha \sin \theta - p \cos \theta)E_y$, $\theta = \theta_u - \theta_l$, and $\theta_i = \arg(\lambda_{Zi})$.

We use a Schrieffer-Wolff transformation to obtain the coupling between states $|+\rangle$ and $|-\rangle$. Expanding to first order in $\eta_l = \varepsilon_{Zl}/(\varepsilon_l - \varepsilon_u)$ and $\eta_u = \varepsilon_{Zu}/(\varepsilon_l - \varepsilon_u)$ and grouping terms according to powers in the electric fields E_1 and E_2 , we obtain

$$\tilde{H}_{-+}^{(2)} = \frac{2\varepsilon_{Zu} \text{Re}(Z_1^* Z_2)}{(\varepsilon_l - \varepsilon_u)^2} + \frac{2\text{Re}(E_2^* Z_1 + E_1^* Z_2)}{\varepsilon_l - \varepsilon_u} + \frac{2\varepsilon_{Zu} \text{Re}(E_1^* E_2)}{(\varepsilon_l - \varepsilon_u)^2}. \quad (\text{A16})$$

The term proportional to $E_2^* Z_1 + E_1^* Z_2$ is linear in the electric field and defines the electric dipole spin resonance term. Substituting Z_1 , Z_2 , E_1 and E_2 we obtain the EDSR matrix element

$$(\tilde{H}_{E_{\parallel}})_{-+}^{(2)} = E_{\parallel} \frac{\varepsilon_{Z0}}{\varepsilon_l - \varepsilon_u} (\alpha \cos(\theta_o - \theta_{\parallel}) + p \sin(\theta_o - \theta_{\parallel})) \quad (\text{A17})$$

where we have assumed an in-plane microwave field of the form $\mathbf{E}_{\parallel} = E_{\parallel}(\hat{\mathbf{x}} \cos(\theta_{\parallel}) + \hat{\mathbf{y}} \sin(\theta_{\parallel}))$.

E. Phonon-induced spin relaxation

The relaxation from $|n'\rangle$ to $|n\rangle$ via emission of a phonon with energy $\hbar\omega_{qs} = \hbar v_s q_s$ can be determined

from Fermi's golden rule,

$$\frac{1}{T_{n \rightarrow n'}} = \frac{2\pi}{\hbar} \sum_{i,j,s,\mathbf{q}_s} |\langle n', n_{\mathbf{q}} + 1 | H_{\varepsilon ijs} | n, n_{\mathbf{q}} \rangle|^2 \times \delta(E_n - E'_n - \hbar\omega_{qs}) \quad (\text{A18})$$

where $s = \ell, t_1, t_2$ are the phonon polarizations, \mathbf{q}_s is the phonon wavevector, and $\sum_{i,j} H_{\varepsilon ijs} = \sum_{i,j} D_{ij} \varepsilon_{ijs}$ is the electron-phonon interaction, and $n_{\mathbf{q}}$ is the phonon population. The deformation potential matrices D_{ij} are determined from the Bir-Pikus Hamiltonian

$$\begin{aligned} \sum D_{ij} \varepsilon_{ijs} = & a'(\varepsilon_{xxs} + \text{c.p.}) \\ & + b'[(J_x^2 - \frac{5}{4}I)\varepsilon_{xxs} + \text{c.p.}] \\ & + (2d'/\sqrt{3})[\{J_x, J_y\}\varepsilon_{xys} + \text{c.p.}] \end{aligned} \quad (\text{A19})$$

where a' , b' , and d' are Bir-Pikus deformation potentials^{29,30} and the strain $\varepsilon_{ijs} = \frac{1}{2}(\partial\delta R_{is}/\partial r_j + \partial\delta R_{js}/\partial r_i)$ of the phonon polarization s is determined by the displacement⁵⁸

$$\delta \mathbf{R}_s = (-i) \sqrt{\frac{\hbar}{2NV\rho\omega_{qs}}} \hat{\mathbf{e}}_{qs} (a_{\mathbf{q}_s}^\dagger + a_{\mathbf{q}_s}) \exp(i\mathbf{q}_s \cdot \mathbf{r}), \quad (\text{A20})$$

where $\hat{\mathbf{e}}_{qs}$ is the normalized phonon polarization vector⁵⁹, N is the number of unit cells, V is the unit cell volume, $NV = L^3$ is the crystal volume, ρ is the mass density, and $a_{\mathbf{q}_s}^\dagger$ ($a_{\mathbf{q}_s}$) creates (destroys) a phonon of wavevector \mathbf{q}_s and polarization s . For $\langle n' | D_{ij} \exp(i\mathbf{q} \cdot \mathbf{r}) | n \rangle$ we use the dipole approximation $\langle n' | D_{ij} (1 + i\mathbf{q} \cdot \mathbf{r} + \dots) | n \rangle \approx \langle n' | D_{ij} | n \rangle$, which is appropriate since $qa \sim 10^{-2}$ where q is the the phonon wavevector and $a \sim 1$ nm is the Bohr radius. At low temperatures $T \ll \hbar\omega/k \approx 0.7$ K we obtain

$$\frac{1}{T_1} = \frac{(\hbar\omega)^3}{20\hbar^4\pi\rho} \left[\sum_i |\langle n' | D_{ii} | n \rangle|^2 \left(\frac{2}{v_l^5} + \frac{4}{3v_t^5} \right) + \sum_{i \neq j} |\langle n' | D_{ij} | n \rangle|^2 \left(\frac{2}{3v_l^5} + \frac{1}{v_t^5} \right) \right] \quad (\text{A21})$$

where v_l and v_t are the longitudinal and transverse sound velocities. For our qubit, the relaxation from $|+\rangle$ to $|-\rangle$ can be evaluated using a Schrieffer-Wolff transformation of the non-diagonal elements of $\tilde{H} = \tilde{H}_{\text{op}} + \tilde{H}_{\varepsilon ijs}$, where $\tilde{H}_{\varepsilon ijs} = U_{t0}^\dagger (\sum_{i,j,s} H_{\varepsilon ijs} \varepsilon_{ijs}) U_{t0}$. We follow the same procedure as Appendix ID to determine the coupling to lowest order in \tilde{H}_{Z0} and $\tilde{H}_{\varepsilon ijs}$ while treating $H_{E,\text{ion}}$, H_{if} and H_E exactly within the 4×4 subspace. We obtain

$$\frac{1}{T_1} = \frac{(\hbar\omega)^3}{20\hbar^4\pi\rho} \left(\frac{\hbar\omega}{4pE_z} \right)^2 \left[\frac{9}{32} b'^2 \left(\frac{2}{v_l^5} + \frac{4}{3v_t^5} \right) + \frac{5}{16} d'^2 \left(\frac{2}{3v_l^5} + \frac{1}{v_t^5} \right) \right] \quad (\text{A22})$$

at the sweet spot. For comparison, we also evaluated the phonon-mediated transition rate from the first excited

level $|\frac{1}{2}\rangle$ to the ground state $|\frac{3}{2}\rangle$ in bulk unstrained silicon, which is allowed even in zero magnetic field, since $|\frac{1}{2}\rangle$ and $|\frac{3}{2}\rangle$ are not time-reversal symmetric. For B_0 along [001] directions we obtain

$$\frac{1}{T_1} = \frac{(\hbar\omega)^3}{20\rho\pi\hbar^4} \left(\frac{1}{v_t^5} + \frac{2}{3v_l^5} \right) 2d'^2, \quad (\text{A23})$$

in agreement with the low-temperature result in ref. 16.

F. Dephasing from electric field fluctuations

In ref. 26, dephasing of spin-orbit qubits was studied due to electric field noise produced by fluctuations in tunneling two-level systems and the occupation of charge traps⁵⁷. The latter were found to dominate dephasing, and are studied here.

First, we note that a charge trap can only fluctuate when it is in tunneling proximity to carrier reservoir or gate. We assume the defect is 1 nm from a gate, so that together with its image in the gate a dipole potential

$$V_d = \frac{ed \cos(\phi)}{4\pi\epsilon R^2} \quad (\text{A24})$$

is produced, where \mathbf{R} is the displacement of the dipole from the acceptor, and ϕ is the angle subtended by the dipole axis and \mathbf{R} , and the dipole distance is $d = 2$ nm. We evaluate the electric field $\delta\mathbf{E} = -\nabla V_d = \hat{\mathbf{x}}\delta E_x + \hat{\mathbf{z}}\delta E_z$ for a dipole displaced along $\hat{\mathbf{x}}$ by 40 nm, and along $\hat{\mathbf{z}}$ by a few nm.

The change $\delta\hbar\omega$ of the Larmor frequency was calculated using the analytic 4×4 model of the main text: δE_x couples off-diagonally through H_E and $H_{E,\text{ion}}$, and δE_z couples diagonally in H_{E_z} and off-diagonally via $H_{E,\text{ion}}$.

G. Numerical Kohn Luttinger Calculations

All theory predictions in the main text were compared with a numerical solution of the acceptor Hamiltonian including the full spatial dependence of $H(\mathbf{k})$. The Hamiltonian $H = H_{\text{LK}} + H_{E,\text{ion}}$, where $H_{\text{LK}} = H(\mathbf{k}) + H_\epsilon + H_{\text{ion}}(\mathbf{r}) + H_{\text{if}}(z) + H_E + H_Z$, was computed in the 6×6 representation of valence band Bloch states $|J, m_J\rangle$ ³⁹, $|\psi_{m_j}\rangle = \sum_{J, m_J} F_{J, m_J}(\mathbf{r}) |J, m_J\rangle$, where $F_{J, m_J}(\mathbf{r})$ are envelope functions. The first step is to numerically diagonalize H_{LK} using $H(\mathbf{k}) =$

$$\begin{pmatrix} P+Q & -S & R & 0 & -\frac{1}{\sqrt{2}}S & \sqrt{2}R \\ -S^\dagger & P-Q & 0 & S & -\sqrt{2}R & \sqrt{\frac{3}{2}}S \\ R^\dagger & 0 & P-Q & S & \sqrt{\frac{3}{2}}S^\dagger & \sqrt{2}Q \\ 0 & R^\dagger & S^\dagger & P+Q & -\sqrt{2}R^\dagger & -\frac{1}{\sqrt{2}}S^\dagger \\ -\frac{1}{\sqrt{2}}S^\dagger & -\sqrt{2}Q & \sqrt{\frac{3}{2}}S & -\sqrt{2}R & P+\Delta_{\text{SO}} & 0 \\ \sqrt{2}R & \sqrt{\frac{3}{2}}S^\dagger & \sqrt{2}Q & -\frac{1}{\sqrt{2}}S & 0 & P+\Delta_{\text{SO}} \end{pmatrix} \quad (\text{A25})$$

in the $|\frac{3}{2}, \frac{3}{2}\rangle, |\frac{3}{2}, \frac{1}{2}\rangle, |\frac{3}{2}, -\frac{1}{2}\rangle, |\frac{3}{2}, -\frac{3}{2}\rangle, |\frac{1}{2}, \frac{1}{2}\rangle, |\frac{1}{2}, -\frac{1}{2}\rangle$, basis, with

$$P = \frac{\hbar^2}{2m_0} \gamma_1 (k_x^2 + k_y^2 + k_z^2), \quad (\text{A26})$$

$$Q = \frac{\hbar^2}{2m_0} \gamma_2 (k_x^2 + k_y^2 - 2k_z^2), \quad (\text{A27})$$

$$R = \frac{\hbar^2}{2m_0} \sqrt{3} (-\gamma_2 (k_x^2 - k_y^2) + 2i\gamma_3 k_x k_y), \quad (\text{A28})$$

$$S = \frac{\hbar^2}{2m_0} 2\sqrt{3} \gamma_3 (k_x - ik_y) k_z, \quad (\text{A29})$$

$H_{\text{ion}}(\mathbf{r}) = -e^2/4\pi\epsilon r$, $H_E = -eE_z z$, $H_{\text{if}} = U_0\Theta(-z)$ with $U_0 \rightarrow \infty$ (using a Dirichlet boundary condition), and H_Z and H_ϵ from the main text. Here, $k_x = i\frac{\partial}{\partial x}$, $k_y = i\frac{\partial}{\partial y}$, $k_z = i\frac{\partial}{\partial z}$, and ϵ_{ij} are the strains. The dielectric constant $\epsilon = 11.4\epsilon_0$, LK parameters $\gamma_1 = 4.28$, $\gamma_2 = 0.375$ and $\gamma_3 = 1.44$, and $\Delta_{\text{SO}} = 44$ meV, Bir-Pikus deformation potentials $b' = -1.42$ eV and $d' = -3.7$ eV, and Lande g-factors $g_1 = 1.07$ and $g_2 = 0.033$ were obtained from the literature^{36,60-62}. The hydrostatic deformation potential a' is not needed since it acts on the valence bands with an identity operator.

The Hamiltonian H_{LK} was diagonalized by finite differences in Cartesian coordinates for different fields E_z and acceptor depths d , to obtain the eigen-energies (eigenstates) $\epsilon_{\text{LK}} (|\Psi_{\text{LK}}\rangle)$ of H_{LK} . The inversion asymmetry-induced mixing of states outside the 4×4 subspace is explicitly included. The effect of the T_d symmetry terms is absent in $|\Psi_{\text{LK}}\rangle$ because the local field of the ion is only present in the unit cell containing the ion, which lies outside the validity of the LK approach^{29,30}.

The T_d symmetry term was included in the spectrum and eigenstates by diagonalizing $H_{\text{LK}} + H_{E,\text{ion}}$ in the basis $|\Psi_{\text{LK}}\rangle$. The p values in $H_{E,\text{ion}}$ were taken to reproduce LH-HH couplings, which are known from experiments³⁶. We also included a multiplicative prefactor \mathcal{F} from the numerics to account for changes in the charge in density at the ion in $|\Psi_{\text{LK}}\rangle$, due to the interface and gate field.

We diagonalized $H_{\text{LK}} + H_{E,\text{ion}}$ using the first 8 states from H_{LK} . We note that states 5 and 6 contribute very little; even though these predominantly split-off hole states have a non-zero density at the ion (non-zero T_d symmetry correction), they are already 20 meV away (compared to the ~ 0.2 meV HH-LH level splitting). The even higher energy states 7 and higher may be neglected *a priori* at low fields, since their principal quantum number is 2 or higher, and the density at the ion and local field coupling is essentially zero.

1. $H_{\text{if}} + H_E$: symmetry and parameters for analytic model

The states $|\Psi_{\text{LK}}\rangle$ experience inversion asymmetry due to explicit presence of the interface and gate field. We have verified that inversion asymmetry-induced mixing of excited states into the 4×4 subspace does not modify the symmetry of H_E from the form in the main

text, for different acceptor depths, by evaluating $H_E = \langle \Psi_{m'_j, \text{LK}} | e\delta\mathbf{E} \cdot \mathbf{r} | \Psi_{m_j, \text{LK}} \rangle$ using the eigenstates of acceptors in static fields E_z of $\Psi_{m_j, \text{LK}}$ in the main text, and fields $\delta\mathbf{E}$ for all three orthogonal directions. Values for $\Delta_{\text{if}} + \Delta(E_z)$ were obtained from eigen-energies, while values of α were obtained from the off-diagonal elements coupling the LH and HH blocks.

2. Larmor frequency and EDSR: numerical results

The LH-HH mixing caused by p in $H_{E, \text{ion}}$ changes the Larmor frequency $\hbar\omega$ of $|\Psi_{\pm}\rangle$ considerably from $|\Psi_{\pm\text{LK}}\rangle$. Numerical calculations of $\hbar\omega$ (Fig. 2C,D, blue squares)

are in agreement with the approximate (Fig. 2C,D, black lines) and analytic solutions (Fig. 2C,D, green lines) to the 4×4 model. In particular, our numerical calculations show that mixing of states outside the 4×4 subspace, and the inclusion of cubic Lande g-factor g_2 with values obtained in experiments, does not qualitatively change the behaviour of the Zeeman energy, showing that it is dominated by the LH-HH mixing inside the 4×4 subspace. The numerical results for EDSR (Fig. 2E,F, orange squares) were obtained by transforming our numerical representations of H_E and $H_{E, \text{ion}}$ into the basis of H , using $\langle \Psi_{\pm} | e\mathbf{E} \cdot \mathbf{r} | \Psi_{\pm} \rangle = U'^{\dagger} (H_E + H_{E, \text{ion}}) U'$, where U' is the unitary matrix that diagonalizes $H_{\text{LK}} + H_{E, \text{ion}}$ in the basis $|\Psi_{\text{LK}}\rangle$.

-
- ¹ D. Loss and D. P. DiVincenzo, Phys. Rev. A **57**, 120 (1998).
- ² B. E. Kane, Nature **393**, 133 (1998).
- ³ J. R. Petta, A. C. Johnson, J. M. Taylor, E. A. Laird, A. Yacoby, M. D. Lukin, C. M. Marcus, M. P. Hanson, and A. C. Gossard, Science **309**, 2180 (2005).
- ⁴ H. Bluhm, S. Foletti, I. Neder, M. Rudner, D. Mahalu, V. Umansky, and A. Yacoby, Nature Physics **7**, 109 (2010).
- ⁵ M. D. Shulman, O. E. Dial, S. P. Harvey, H. Bluhm, V. Umansky, and A. Yacoby, Science **336**, 202 (2012).
- ⁶ J. T. Muhonen, J. P. Dehollain, A. Laucht, F. E. Hudson, R. Kalra, T. Sekiguchi, K. M. Itoh, D. N. Jamieson, J. C. McCallum, A. S. Dzurak, and A. Morello, Nature Nanotech **9**, 986 (2014).
- ⁷ M. Veldhorst, J. C. C. Hwang, C. H. Yang, A. W. Leenstra, B. de Ronde, J. P. Dehollain, J. T. Muhonen, F. E. Hudson, K. M. Itoh, A. Morello, and A. S. Dzurak, Nature Nanotech **9**, 981 (2014).
- ⁸ X. Hu and S. Das Sarma, Phys. Rev. Lett. **96**, 100501 (2006).
- ⁹ D. Culcer, X. Hu, and S. Das Sarma, Applied Physics Letters **95**, 073102 (2009).
- ¹⁰ V. N. Golovach, M. Borhani, and D. Loss, Phys. Rev. B **74**, 165319 (2006).
- ¹¹ C. Flindt, A. S. Sørensen, and K. Flensberg, Phys. Rev. Lett. **97**, 240501 (2006).
- ¹² D. Bulaev and D. Loss, Phys. Rev. Lett. **98**, 097202 (2007).
- ¹³ M. Trif, V. N. Golovach, and D. Loss, Phys. Rev. B **77**, 045434 (2008).
- ¹⁴ A. Pályi, P. R. Struck, M. Rudner, K. Flensberg, and G. Burkard, Phys. Rev. Lett. **108**, 206811 (2012).
- ¹⁵ C. Kloeffel, M. Trif, P. Stano, and D. Loss, Phys. Rev. B **88**, 241405 (2013).
- ¹⁶ R. Ruskov and C. Tahan, Phys. Rev. B **88**, 064308 (2013).
- ¹⁷ K. C. Nowack, F. H. L. Koppens, Y. V. Nazarov, and L. M. K. Vandersypen, Science **318**, 1430 (2007).
- ¹⁸ S. Nadj-Perge, S. M. Frolov, E. P. A. M. Bakkers, and L. P. Kouwenhoven, Nature **468**, 1084 (2010).
- ¹⁹ K. D. Petersson, L. W. McFaul, M. D. Schroer, M. Jung, T. J. MM, A. A. Houck, and J. R. Petta, Nature **490**, 380 (2012).
- ²⁰ V. S. Pribiag, S. Nadj-Perge, S. M. Frolov, J. W. G. van den Berg, I. van Weperen, S. R. Plissard, E. P. A. M. Bakkers, and L. P. Kouwenhoven, Nature Nanotech **8**, 170 (2013).
- ²¹ J. Medford, J. Beil, J. M. Taylor, E. I. Rashba, H. Lu, A. C. Gossard, and C. M. Marcus, Phys. Rev. Lett. **111**, 050501 (2013).
- ²² X. Hu, Y.-x. Liu, and F. Nori, Phys. Rev. B **86**, 035314 (2012).
- ²³ J. M. Taylor, V. Srinivasa, and J. Medford, Phys. Rev. Lett. **111**, 050502 (2013).
- ²⁴ Z.-L. Xiang, S. Ashhab, J. You, and F. Nori, Rev. Mod. Phys. **85**, 623 (2013).
- ²⁵ P. Huang and X. Hu, Phys. Rev. B **89**, 195302 (2014).
- ²⁶ A. Bermeister, D. Keith, and D. Culcer, Applied Physics Letters **105**, 192102 (2014).
- ²⁷ J. Koch, T. M. Yu, J. Gambetta, A. A. Houck, D. I. Schuster, J. Majer, A. Blais, M. H. Devoret, S. M. Girvin, and R. J. Schoelkopf, Phys. Rev. A **76**, 042319 (2007).
- ²⁸ J. Majer, J. M. Chow, J. M. Gambetta, J. Koch, B. R. Johnson, J. A. Schreier, L. Frunzio, D. I. Schuster, A. A. Houck, A. Wallraff, A. Blais, M. H. Devoret, S. M. Girvin, and R. J. Schoelkopf, Nature **449**, 443 (2007).
- ²⁹ G. L. Bir, E. I. Butikov, and G. E. Pikus, Surface Science **24**, 1467 (1963).
- ³⁰ G. L. Bir, E. I. Butikov, and G. E. Pikus, Surface Science **24**, 1475 (1963).
- ³¹ M. Trif, V. N. Golovach, and D. Loss, Phys. Rev. B **75**, 085307 (2007).
- ³² A. Blais, R.-S. Huang, A. Wallraff, S. Girvin, and R. Schoelkopf, Phys. Rev. A **69**, 062320 (2004).
- ³³ A. Wallraff, D. I. Schuster, A. Blais, L. Frunzio, R. S. Huang, J. Majer, S. Kumar, S. M. Girvin, and R. J. Schoelkopf, Nature **431**, 162 (2004).
- ³⁴ E. A. Chekhovich, M. M. Glazov, A. B. Krysa, M. Hopkinson, P. Senellart, A. Lemaître, M. S. Skolnick, and A. I. Tartakovskii, Nature Physics **9**, 74 (2012).
- ³⁵ A. M. Tyryshkin, S. Tojo, J. J. L. Morton, H. Riemann, N. V. Abrosimov, P. Becker, H.-J. Pohl, T. Schenkel, M. L. W. Thewalt, K. M. Itoh, and S. A. Lyon, Nature Materials **11**, 143 (2011).
- ³⁶ A. Köpf and K. Lassmann, Phys. Rev. Lett. **69**, 1580 (1992).
- ³⁷ L. Calvet, R. Wheeler, and M. Reed, Phys. Rev. Lett. **98** (2007).
- ³⁸ B. Golding and M. I. Dykman, arxiv:0309147 (2003).
- ³⁹ J. Luttinger and W. Kohn, Phys. Rev. **97**, 869 (1955).

- ⁴⁰ S. G. Pavlov, N. Deßmann, V. N. Shastin, R. K. Zhukavin, B. Redlich, A. F. G. van der Meer, M. Mittendorff, S. Wimmerl, N. V. Abrosimov, H. Riemann, and H. W. Hübers, *Phys. Rev. X* **4**, 021009 (2014).
- ⁴¹ A. Baldereschi and N. Lipari, *Phys. Rev. B* **8**, 2697 (1973).
- ⁴² R. Winkler, “Spin-orbit coupling effects in two-dimensional electron and hole systems”, Springer Tracts in Modern Physics, Vol. 191 (Springer Berlin Heidelberg, Berlin, Heidelberg, 2003).
- ⁴³ C. Chao and S. Chuang, *Phys. Rev. B* **46**, 4110 (1992).
- ⁴⁴ J. A. Mol, J. Salfi, R. Rahman, Y. Hsueh, J. A. Miwa, G. Klimeck, M. Y. Simmons, and S. Rogge, *Applied Physics Letters* **106**, 203110 (2015).
- ⁴⁵ J. van der Heijden, J. Salfi, J. A. Mol, J. Verduijn, G. C. Tettamanzi, A. R. Hamilton, N. Collaert, and S. Rogge, *Nano Lett.* **14**, 1492 (2014).
- ⁴⁶ C. C. Lo, M. Urdampilleta, P. Ross, M. F. Gonzalez-Zalba, J. Mansir, S. A. Lyon, M. L. W. Thewalt, and J. J. L. Morton, *Nature Publishing Group* **14**, 490 (2015).
- ⁴⁷ H. Neubrand, *Phys. Status Solidi (b)* **86**, 269 (1978).
- ⁴⁸ G. Smit, S. Rogge, J. Caro, and T. Klapwijk, *Phys. Rev. B* **70** (2004).
- ⁴⁹ J. Schrieffer and P. Wolff, *Phys. Rev.* **149**, 491 (1966).
- ⁵⁰ A. Morello, J. J. Pla, F. A. Zwanenburg, K. W. Chan, K. Y. Tan, H. Huebl, M. Möttönen, C. D. Nugroho, C. Yang, J. A. van Donkelaar, A. D. C. Alves, D. N. Jamieson, C. C. Escott, L. C. L. Hollenberg, R. G. Clark, and A. S. Dzurak, *Nature* **467**, 687 (2010).
- ⁵¹ K. D. Petersson, C. G. Smith, D. Anderson, P. Atkinson, G. A. C. Jones, and D. A. Ritchie, *Nano Lett.* **10**, 2789 (2010).
- ⁵² J. Salfi, J. A. Mol, R. Rahman, G. Klimeck, M. Y. Simmons, L. C. L. Hollenberg, and S. Rogge, arxiv:1507.06125 (2015).
- ⁵³ J. Salfi, J. A. Mol, R. Rahman, G. Klimeck, M. Y. Simmons, L. C. L. Hollenberg, and S. Rogge, *Nature Materials* **13**, 605 (2014).
- ⁵⁴ B. Koiller, X. Hu, and S. Das Sarma, *Phys. Rev. Lett.* **88**, 027903 (2001).
- ⁵⁵ S. E. de Graaf, A. V. Danilov, A. Adamyan, T. Bauch, and S. E. Kubatkin, *Journal of Applied Physics* **112**, 123905 (2012).
- ⁵⁶ S. E. de Graaf, D. Davidovikj, A. Adamyan, S. E. Kubatkin, and A. V. Danilov, *Applied Physics Letters* **104**, 052601 (2014).
- ⁵⁷ E. Paladino, Y. M. Galperin, G. Falci, and B. L. Altshuler, *Rev. Mod. Phys.* **86**, 361 (2014).
- ⁵⁸ G. P. Srivastava, *Physics of Phonons* (Adam Hilger, New York, 1990).
- ⁵⁹ H. Ehrenreich and A. W. Overhauser, *Phys. Rev.* **104**, 331 (1956).
- ⁶⁰ H. Neubrand, *Phys. Status Solidi (b)* **90**, 301 (1978).
- ⁶¹ P. Lawaetz, *Phys. Rev. B* **4**, 3460 (1971).
- ⁶² J. Bernholc and S. Pantelides, *Phys. Rev. B* **15**, 4935 (1977).